ChemCatChem

Research Article
doi.org/10.1002/cctc.202401893

Chemistry Europe
European Chemical Societies Publishing

www.chemcatchem.org

Linkers in Action: Exploring Fusion Enzymes for Oxyfunctionlizations in Non-Conventional Media Through Experiments and Simulations

Yu Ma,[a] Jan Philipp Bittner,[b] Guillem Vernet,[c] Ningning Zhang,*[c] and Selin Kara*[a, c]

Baeyer–Villiger monooxygenases (BVMOs) are key for the selective oxidation of ketones into diverse (cyclic) esters. However, challenges like oxygen and cofactor dependence and substrate/product inhibition hinder their broader application. To address some of these issues, nonconventional media have been applied; still, they lack certain water required for enzyme hydration and cofactor regeneration, reducing activity and/or stability. Fusion approaches enable efficient cofactor recycling by shortening the diffusion distance between enzyme active sites in cascades, especially under low-water conditions. Trial-and-error linker design and time-intensive construction of fusion enzymes substantially slow down the development of fusion enzymes. In this study, we present the work on the fusions of cyclohexanone monooxygenase (CHMO) and alcohol dehydrogenase (ADH) with linkers owing varying lengths and flexibility in both orientations in nonconventional media, focusing on understanding the effects of linkers on the structural and catalytic properties of fusion enzymes. As such, 12 new fusion enzymes were constructed and evaluated regarding the kinetics, specific activity, and stability, identifying the optimal ones for the linear oxyfunctionlization cascade in aqueous–organic biphasic systems. The conformation and flexibility of linkers and the spatial arrangement of fusion enzymes were studied with simulations, which provides a deep understanding of linkers' influence and offers insights into the rational design of fusion enzymes.

1. Introduction

Multienzymatic cascades represent a significant advancement in chemical synthesis, offering a sustainable and efficient alternative to traditional methods by mimicking natural biosynthesis with enzymes.[1–3] These biocatalytic reactions often involve oxidoreductases like Baeyer–Villiger monooxygenases (BVMOs) for facilitating selective oxidation reactions to synthesize valuable bioactive compounds or chiral precursors.[4–6] However, using BVMOs encounters several challenges, chief among them being their reliance on costly cofactors (i.e., nicotinamide adenine dinucleotide phosphate (NADPH), the need for efficient provision of oxygen, and enzyme instability.[7,8] Moreover, their practical use in aqueous media faces several limitations related to product autohydrolysis, low oxygen solubility, and substrate and product inhibition issues.

The use of nonconventional media for biocatalytic transformations emerges as a promising solution.[9–12] This approach has been proven to accommodate high substrate loadings,[13] enhance oxygen supply,[14] and reduce the ecological footprint (i.e., low values of E-factor),[15,16] thereby contributing significantly to sustainability. However, employing BVMO-based reactions under nonconventional conditions brings about its own set of challenges. One primary obstacle is the need for a minimum amount of water to facilitate the diffusion of water-soluble nicotinamide cofactors between the active sites of cascading enzymes.[17] Additionally, BVMOs exhibit relatively low stability when exposed to high concentrations of organic solvents,[18] further complicating their implementation in non-aqueous environments.

To address these challenges, a promising strategy lies in utilizing fusion enzymes. Specifically, when dealing with cofactor-dependent enzymes, the fused form can effectively shorten the transport distance between the active sites of enzymes,[19,20] simultaneously reducing the detrimental impact of organic solvents on nicotinamide cofactors.[21] Furthermore, this approach can improve enzyme stability and catalytic efficiency, while facilitating the establishment of self-sufficient in situ cofactor regeneration systems.[22] The feasibility of employing fused enzymes has been widely demonstrated in aqueous media.[19,23,24] Until recently, the use of fused oxygenat-

[a] Y. Ma, Prof. Dr. S. Kara
Biocatalysis and Bioprocessing Group, Department of Biological and Chemical Engineering, Aarhus University, Gustav Wieds Vej 10, Aarhus 8000, Denmark
E-mail: selin.kara@iftc.uni-hannover.de

[b] J. P. Bittner
Institute of Thermal Separation Processes, Hamburg University of Technology, Eißendorfer Straße 38, Hamburg 21073, Germany

[c] G. Vernet, Dr. N. Zhang, Prof. Dr. S. Kara
Institute of Technical Chemistry, Leibniz University Hannover, Callinstraße 5, Hannover 30167, Germany
E-mail: ningning.zhang@iftc.uni-hannover.de

Supporting information for this article is available on the WWW under https://doi.org/10.1002/cctc.202401893

ing enzymes in low-water conditions has been on the rise. Huang et al.[25] reported the first application of a fused type II flavin-containing monooxygenase (FMO-E) and horse liver alcohol dehydrogenase (HLADH) with a flexible linker in diverse organic solvents containing 5 vol.% buffer for the synthesis of γ-butyrolactone. In another example, Mourelle-Insua et al.[26] achieved about 10% conversion with a fusion of formate dehydrogenase from *Burkholderia stabilis* (*Bs*FDH) and cyclohexanone monooxygenase from *Thermocrispum municipale* (*Tm*CHMO) in 1 vol.% 1,4-dioxane, while fusing phosphite dehydrogenase from *Pseudomonas stutzeri* (*Ps*PTDH) with *Tm*CHMO through short–flexible linkers resulted in a full conversion. This underscores the profound influence of linker design on the catalytic performance of fusion enzymes in defined reaction systems. Recently, Vernet et al.[17] documented the use of the fusion enzyme *Tb*ADH-*Tm*CHMO (ADH from *Thermoanaerobacter brockii*) with a flexible linker as cross-linked enzyme aggregates (CLEAs) in cyclopentyl methyl ether (CPME) and methyl *tert*-butyl ether (MTBE) containing $\leq$5 vol.% buffer, showing promising operational and storage stability. A recent work by us successfully demonstrated the first use of fusion enzymes *Tb*ADH-*Tm*CHMO in deep eutectic solvents. [27] Although these studies highlight the great potential of employing fusion enzymes in organic media, only a limited number of fusion enzymes have been explored. The dynamism and effects of fusion enzyme systems in such environments remain gaps in our knowledge.

Most fusion enzymes are generated through a genetic approach, where linker peptides are pivotal in binding target proteins.[28–30] The presence of linkers allows for the separation of two enzymes and thus avoids mutual interference during protein folding and catalysis.[28,29,31] There are at least two factors to consider when designing a fusion enzyme: 1) which type of linker to use and 2) in which order proteins should be placed. For the first aspect, the composition and length of a linker are the two determining factors of its physicochemical properties (flexibility vs rigidity, and hydrophilicity vs hydrophobicity). They can highly affect the spatial distribution of fused subunits. Many studies demonstrated that fusion enzymes using various linkers can offer catalytic benefits such as higher product yields, improved catalytic activity, and stability, but these advantages are not always consistent across all fusion combinations.[30,32,33] Some studies even showed a decrease in enzyme activity or stability.[20,26] In addition to these inconsistencies, linker design has been a time-consuming trial-and-error approach, which slows down the development of fusion enzymes. Therefore, to simplify the generation of fusion enzymes, it's crucial to understand how the order of enzymes and the selection of linkers affect their catalytic properties, particularly for certain oxidoreductases that are currently under the spotlight, like BVMOs.

To better understand the impact of linkers on fusion enzymes, a combination of experiments and simulations is required to achieve atomic-resolution insights. There have been limited successful attempts to reveal the atomic and molecular-level intricacies of fusion enzymes.[34,35] This challenge is primarily due to the time- and labor-intensive obtention of fusion enzymes, involving multiple tasks (e.g., protein expression, purification, and crystallization). As a complementary, the introduction of AlphaFold2 (DeepMind) represents a ground-breaking advancement, enabling the rapid and precise prediction of protein structure modeling.[36] The capabilities of AlphaFold2 extend beyond single protein structures as it was also used to predict the structures of complex protein assemblies, including those affected by short peptide sequences (e.g., linkers).[37–40] This achievement opens up an opportunity for the present research to gain insights into the conformation of linkers and fusion enzymes.

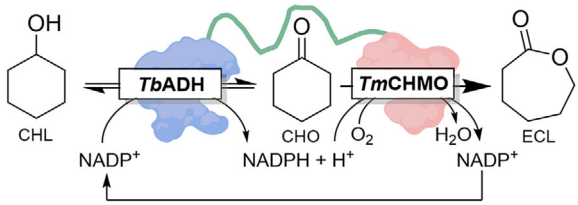

Scheme 1. Design of fused alcohol dehydrogenase (ADH) and cyclohexanone monooxygenase (CHMO) for oxyfunctionlization of cyclohexanol (CHL) to ε-caprolactone (ECL).

Building on the established fusion enzyme *Tb*ADH-*Tm*CHMO with a peptide linker of 14 amino acids,[17,41] we have expanded the collection of innovative fusion enzymes of *Tb*ADH and *Tm*CHMO bridged by various linkers with different lengths and flexibilities to two fusion orientations for the linear oxyfunctionlization cascade of cyclohexanol to ε-caprolactone (Scheme 1). These new fusion enzymes were systematically evaluated regarding stability and activity and applied in the redox-neutral linear cascade reactions first in nonconventional media, specifically aqueous–organic biphasic systems. With the aid of AlphaFold2, the structures of the selected fusion enzymes with superior catalytic performance were predicted. Molecular dynamics (MD) simulations were conducted to gain structural insights into the enzyme conformation, flexibility, and the distance between the active sites of the fusion enzymes. The combination of experimental and computational analyses provided the first comprehensive understanding of the relation between peptide linkers, fusion enzymes, and enzyme catalytic properties, contributing to the rational design of fusion enzymes for biocatalysis.

2. Results and Discussion

2.1. Design and Construction of Fusion Enzymes

The design of efficient and stable fusion enzymes involves carefully considering two key factors: (i) the order in which enzymes are placed and (ii) the characteristics of the linkers employed. Six representative linkers were chosen to bridge *Tb*ADH and *Tm*CHMO, considering the intricate interplay between the linkers and the diverse structures of fusion enzymes. These linkers were identified based on previous research on performance enhancement. Therefore, not all types of linkers are covered. The selected linkers were categorized according to their length, composition,

Table 1. Different linkers used in this study.

Entry	Size	Composition of Linkers	Length	Flexibility	Abbreviation of Linkers	Abbreviation of Fusions	Ref.
1	Small	SRSAAG	6	Flexible	**6F**	Tb-6F-Tm	[42]
						Tm-6F-Tb	
2		WYH	3	Rigid	**3R**	Tb-3R-Tm	[43]
						Tm-3R-Tb	
3		$(WYH)_2$	6	Rigid	**6R1**	Tb-6R1-Tm	/
						Tm-6R1-Tb	
4		WYHHHH	6	Rigid	**6R2**	Tb-6R2-Tm	[43]
						Tm-6R2-Tb	
5		WYHAAA	6	Rigid	**6R3**	Tb-6R3-Tm	[43]
						Tm-6R3-Tb	
6	Medium	SSATGSATGSAG	12	Flexible	**12F**	Tb-12F-Tm	[42]
						Tm-12F-Tb	
7		SSGGSGGSGGSAGT	14	Flexible	**14F**	Tb-14F-Tm	[20, 41]

and flexibility, as outlined in Table 1 (more details in Table S1). Specifically, five small linkers (3–6 amino acid residues) are either flexible or rigid, while two medium-sized linkers (>6 amino acid residues) exhibit flexibility.

In this study, the fusion enzymes are named based on the order of two fusion domains and the corresponding linker, that is, *Tb-linker-Tm* or *Tm-linker-Tb*. The designation of the linker comprises the number (length) of amino acid residues it contains, followed by its flexibility, denoted as either "*F*" for the flexible or "*R*" for the rigid. Sequential labelling was used for the linkers with the same number of amino acids and flexibility (entries 3–5). New fusion enzymes were engineered in two orientations using PCR amplification (Table S2), with their successful construction confirmed through sequencing and subsequent transformation into *Escherichia coli* (*E. coli*) top 10 cells. Fermentation productivity ranged from 7.6 to 21.6 g wet cells per liter culture (Table S3). In addition, the expression of fusion enzymes was determined by SDS-PAGE (Figure S1), which showed a band intensity discrepancy at around 101 kDa. These results indicate the replacement of the linker indeed exerted a discernible influence on enzyme production. Overall, 12 new fusion enzymes were designed and constructed, and Table 1 also contains the Tb-14F-Tm fusion enzyme as a reference for comparison.[41]

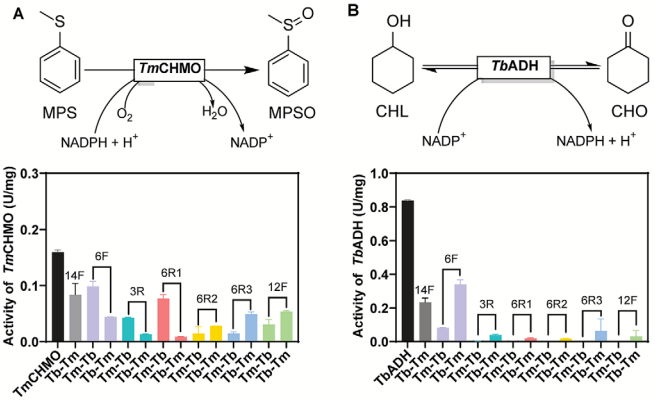

Figure 1. The specific activity of fusion enzymes in cell-free extract (CFE). (A) Activity of CHMO and (B) activity of ADH. Reactions were performed in 1 mL KPi buffer (50 mM, pH 8) containing substrate (0.25 mM thioanisole or 10 mM cyclohexanol), and 0.1 mM NADPH or $NADP^+$ at 25 °C.

2.2. Specific Activity Analysis of Fusion Enzymes

To assess the integrity of *Tb*ADH and *Tm*CHMO in these fusion enzymes, the specific activity of both enzymes in cell-free extract (CFE) was first studied. *Tb*ADH activity was determined with cyclohexanol (CHL) as substrate, whereas *Tm*CHMO activity was measured using thioanisole (MPS) as substrate to avoid ADH cross-reactivity (Figure 1). The activity of CHMO towards thioanisole proved comparable to its activity towards cyclohexanone.[44] All fusion enzymes generally exhibited lower CHMO activities (decreased from 3.8- to 9.4-fold) compared to single *Tm*CHMO. Regarding different fusion directions, no discernible trend in CHMO activity was observed (Figure 1A). Notably, Tm-6F-Tb showed a higher CHMO activity than the original Tb-14F-Tm, implying the potential of link 6F. Conversely, the ADH activity of the fusion enzymes displayed remarkable variations (Figure 1B). A notable difference was observed between N-terminal, which retained ADH activity, and C-terminal ADHs, which showed almost no ADH activity. Specifically, N-terminal ADHs exhibited reduced activity from 2.8- to 13.5-fold compared to single *Tb*ADH. These findings are in line with the previous research that ADH activity was lost when they were fused at C-terminus.[20] Only in the case of Tm-6F-Tb ADH activity could be detected, which is 4-fold lower in comparison to the N-terminal ADH. These observations indicate that ADH is more susceptible to fusion orientation and linker properties than CHMO. After purification, the fusion enzymes retained CHMO activity, but their ADH activity varied (Figure S2). Except for Tb-6R3-Tm, all purified fusion enzymes with rigid linkers lost ADH activity (Figure S2B), further highlighting the instability of ADH post-fusion. Overall, four new fusion enzymes (namely Tm-

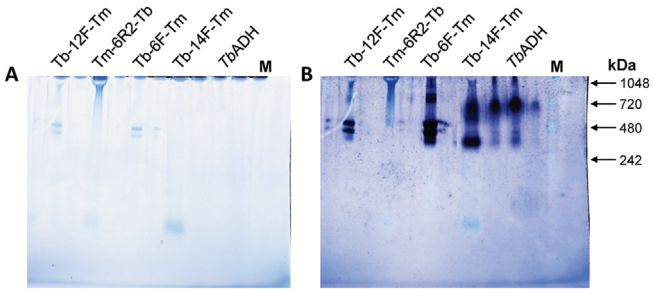

Figure 2. (A) Blue native PAGE (4–15 vol.%) stained with Coomassie, and (B) simultaneous zymography of fusion enzymes.

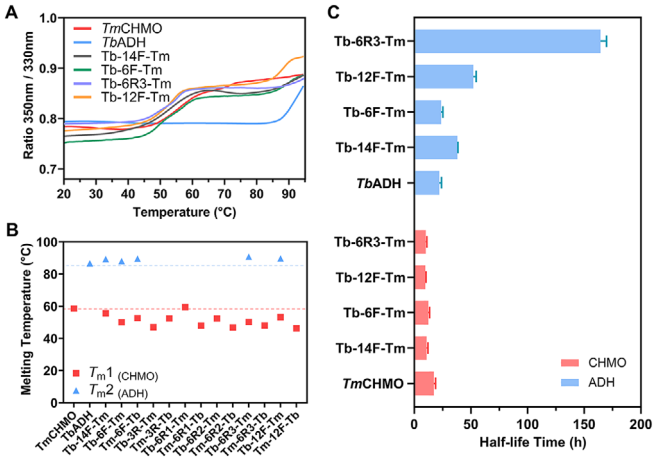

Figure 3. (A) Thermal unfolding curves of *Tm*CHMO, *Tb*ADH, and the selected fusion enzymes. (B) Melting temperature (T_m) of single or fused *Tm*CHMO (red) and *Tb*ADH (blue). (C) Half-life time ($t_{1/2}$) of *Tm*CHMO, *Tb*ADH, and the selected fusion enzymes after incubation in aqueous systems.

6F-Tb, Tb-6F-Tm, Tb-6R3-Tm, and Tb-12F-Tm) were identified as prospective ones for further investigation.

The kinetics of fusion enzymes compared to the reference construct Tb-14F-Tm showed varying catalytic rates (V_{max}) in the range from 0.04 to 0.5 U/mg for CHMO and 0.2 to 3.7 U/mg for ADH (Table S4). Linkers significantly influenced enzyme affinity (K_M values of CHMO ranging from 0.05 to 0.2 mM for thioanisole, and 1.8 to 31.0 mM for cyclohexanol in the case of ADH) and catalytic efficiency (k_{cat}/K_M values ranging from 1.5 to 67.5 mM/min for CHMO and from 0.01 to 113.5 mM/min for ADH). Regarding ADH, although some fusion enzymes showed improved efficiency (e.g., Tb-6F-Tm and Tb-6R3-Tm); others displayed decreased efficiency, notably Tb-12F-Tm due to the increased K_M (Table S4). These results further highlight the significant impact of fusion linkers on catalytic performance and enzyme-substrate interactions, especially for ADHs.

Typically, ADHs are dimeric or tetrameric forms, crucial for enzyme stability and activity.[20] The observed activity reduction for C-terminal ADH can be attributed to the obstruction of oligomerization, a crucial process for ADH functionality.[45,46] To gain insight into the oligomeric behavior of the fusion enzymes, blue native polyacrylamide gel electrophoresis (BN-PAGE) was conducted for several of the more active and the least active (Tm-6R2-Tb) fusion enzymes (Figure 2A). Following BN-PAGE, zymography was performed on the gel to visualize the active ADH as dark purple bands (Figure 2B).

It is postulated that single *Tb*ADH can form active tetramers, resulting in a molecular weight of more than 400 kDa. Except for Tm-6R2-Tb, all other fusion enzymes showing ADH activity are clearly visible from the distinct dark band. Electrophoretic mobility differed among these selected fusion enzymes: Tb-12F-Tm and Tb-6F-Tm showed reduced mobility compared to Tb-14F-Tm, hinting at a distinct structural organization. Interestingly, the absence of a dark purple band for Tb-6R2-Tm signified a profound structural alteration; this fusion enzyme appears to form a "tie-like" larger complex that impedes its migration on the gel. This may indicate an aggregated or oligomeric state different from the expected tetrameric form.

2.3. Stability of Fusion Enzymes in Aqueous Media

To comprehensively assess the impact of linkers on fusion enzymes, the stability defined as melting temperature (T_m) and half-life time ($t_{1/2}$) for purified single enzymes and fusion enzymes were evaluated in KPi buffer (50 mM, pH 8.0) (Figure 3). The single enzymes showed typical transition curves whereas most fusion enzymes displayed two transition points upon protein unfolding as temperature increased (Figure 3A, only selected fusion enzymes were shown), from which T_m values could be derived (Figure 3B). Specifically, the first T_m corresponds to the melting temperature of the *Tm*CHMO domain, while the latter T_m reflects the higher unfolding temperature of *Tb*ADH domain. The single enzymes, *Tm*CHMO and *Tb*ADH, serve as benchmarks with their T_m values noted at 58.6 and 87.7 °C, respectively (Figure 3B). In terms of the first T_m, the single *Tm*CHMO showed the highest T_m value compared to the fusion enzymes, aside from a slight increase in Tm-6R1-Tb at 59.4 °C. Among these fusion enzymes, the longer flexible linkers (Tb-14F-Tm and Tb-12F-Tm) resulted in relatively higher T_m values. As for the second T_m, five fusion enzymes (Tb-14F-Tm, Tb-12F-Tm, Tb-6F-Tm, Tm-6F-Tb, and Tb-6R3-Tm) showed the T_m values for *Tb*ADH at slightly higher temperatures, approximately 88 °C (Figure 3B). Notably, the other six fusion enzymes that did not exhibit the second T_m were the exact fusion enzymes that lost ADH activity upon purification (Figure S2B). This provides further evidence of the pronounced instability shown by *Tb*ADH upon fusion with these specific rigid linkers.

The four fusion enzymes with superior specific activity and T_m were subjected to the half-life time ($t_{1/2}$) analysis before their application in the targeted cascade reaction. In general, the $t_{1/2}$ of ADH is superior to that of CHMO (Figure 3C). Specifically, the fusion enzymes exhibit a diminished stability to single *Tm*CHMO, which aligns with the observed trends concerning specific activity and thermal stability (Figures 1A and 3B). Conversely, the stability of ADH within these fusions has been enhanced by 0.1- to 7.2-fold compared to single *Tb*ADH. In particular, Tb-6R3-Tm demonstrates a remarkably elevated $t_{1/2}$, indicating that the rigid linker is beneficial to the stability of ADH. Moreover, the fusion enzymes employing flexible longer linkers (Tb-14F-Tm and Tb-

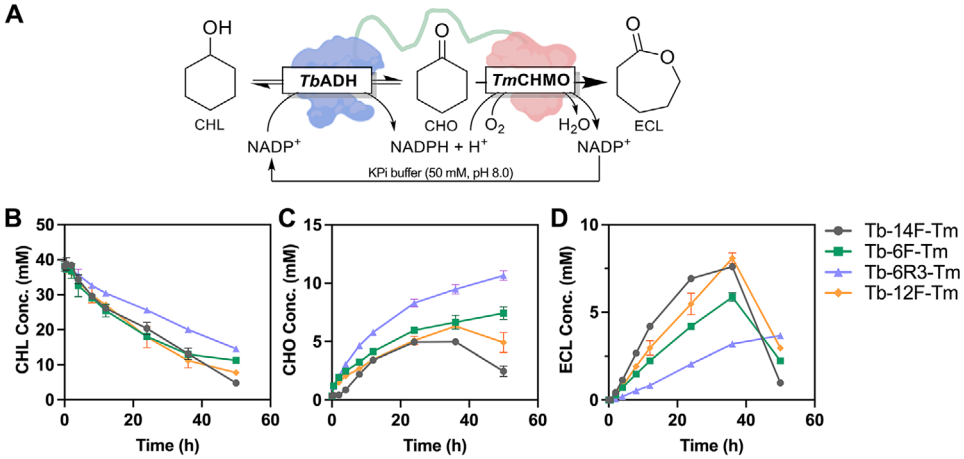

Figure 4. (A) The reaction cascade starting with the oxidation of cyclohexanol (CHL) to cyclohexanone (CHO) and further to ε-caprolactone (ECL) catalyzed by fusion enzymes. Progressive curves of CHL, CHO, and ECL in KPi buffer (B—D). Reaction condition: 2 mL KPi system (50 mM, pH 8.0) or 5 mL biphasic system with 40 mM CHL, 1 mM $NADP^+$, 1 U/mL CHMO activity, and varying ADH activity, at 30 °C and 480 rpm. The results are the average values from independent duplicate experiments.

12F-Tm) exhibit extended half-life times compared to those with flexible shorter linkers (Tb-6F-Tm). This trend is particularly evident for ADH but is precisely the opposite in CHMO. Such an observation could be attributed to the enhanced structural flexibility or spatial accommodation afforded by the longer linkers, which may contribute to the stabilization of the enzyme's active conformation and thus prolong its lifespan.

2.4. The Cascade Reaction of Fusion Enzymes in Aqueous Systems

According to the activity and stability analyses, three fusion enzymes (Tb-12F-Tm, Tb-6F-Tm, and Tb-6R3-Tm) were chosen for further study in the linear cascade, referencing Tb-14F-Tm for comparison. The linear cascade consists of the stepwise oxidation of cyclohexanol (CHL) to cyclohexanone (CHO) and finally to ε-caprolactone (ECL), which is catalyzed by *Tb*ADH and *Tm*CHMO respectively involving a circular consumption and regeneration of $NADP^+$/NADPH (Figure 4A). Given the CHMO-catalyzed reaction is the rate-limiting step,[20] a unified amount of *Tm*CHMO activity (1 U) in CFE was used to have a fair comparison and this resulted in distinct activity ratios for ADH to CHMO for fusion enzymes: 2.2 for Tb-6F-Tm, 1.7 for Tb-6R3-Tm, 0.82 for Tb-14F-Tm, and 0.15 for Tb-12F-Tm. The progressive curves of the substrate (CHL), intermediate (CHO), and product (ECL) are shown in Figure 4. Specifically, the fusion enzymes led to a similar gradual depletion of CHL with a slower decline in Tb-L6R3-Tm, indicating it is less efficient than others (Figure 4B). In terms of CHO accumulation, a different trend was observed as Tb-L6R3-Tm resulted in the highest amount of CHO followed by 6F, 12F, and 14F (Figure 4C). This result indicates the different catalytic activity of CHMO in these fusion enzymes. Correspondently, ECL formation increased steadily in the opposite order of 14F > 12F > 6F > 6R3 (Figure 4D), which was caused by the known inhibitory impact of accumulated CHO on CHMO activity.[6,47] Remarkably, Tb-12F-Tm achieved the highest ECL concentration after 36 h, suggesting its potential as an efficient candidate for the cascade. These results indicate that longer flexible linkers are beneficial to the biocatalytic performance of Tb-Tm. Notably, the decline of ECL concentration, in the end, is due to its auto–hydrolysis to form side product 6-hydroxyhexanoic acid, as proven by a drop in pH from 8.0 to 6.2, which is aligned with the previous research.[17] This subsequently slows down the pH-dependent alcohol oxidation by ADHs as alcohol deprotonation is favored at higher pHs,[20] thus resulting in decreased CHO accumulation.

2.5. Structural Insights into the Selected Fusion Enzymes and MD Simulations

To fully understand the effects of linkers and fusion orientation on the catalytic performance of fusion enzymes, the structures of single *Tm*CHMO and *Tb*ADH, as well as several selected fusion enzymes—the reference (Tb-14F-Tm), the best performing one (Tb-L6F-Tm), the least effective one (Tm-6R2-Tb), and their Tm-Tb counterparts, were predicted via AlphaFold2. These predicted structures were the foundation of molecular dynamics (MD) simulations of the linkers in aqueous solutions to understand the underlying phenomena on the molecular level.

First, the marked difference in the activity of fusion enzymes observed between Tb-Tm and Tm-Tb underlines the significance of enzyme arrangement on the functionality of fusion enzymes. Specifically, CHMO activity was retained in both cases regardless of its position at the C- or N-terminus. This is due to the fact *Tm*CHMO has a monomeric structure, in which both termini are free and exposed to the surrounding solution while the internal active site is safeguarded by the external structural shell (Figure 5A).[44] In contrast, *Tb*ADH functions as a homotetramer and its oligomerization crucially depends on the interactions between the specific structural features of one monomer (β-sheet β12 and α-helix α9) with the corresponding structures of another monomer (Figure 5B).[48,49] These unique structural features of ADH result in a significant difference between Tb-Tm

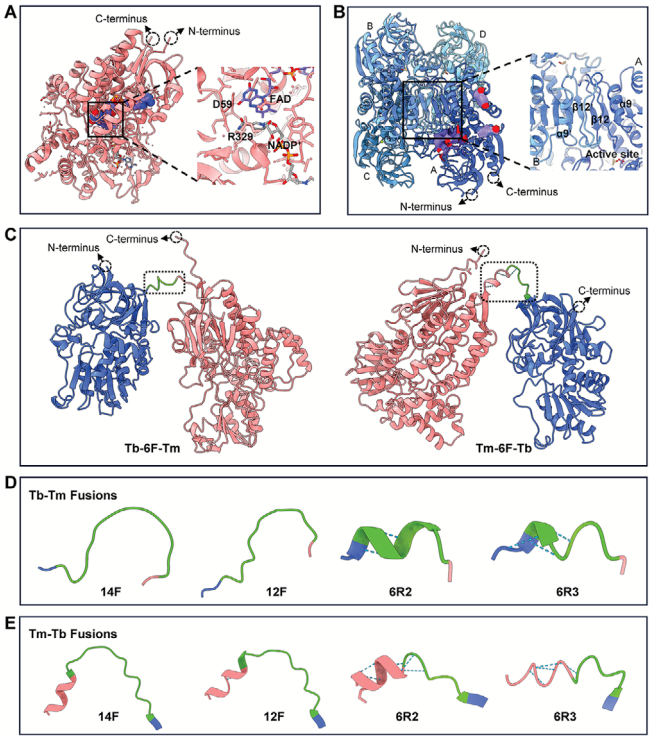

Figure 5. The quaternary structure of (A) *Tm*CHMO (PDB: 5M10) and (B) *Tb*ADH (PDB: 1BZX) showing N- and C-terminus and close-up view of the active site. (C) The predicted quaternary structures of the fusion enzymes using the linker 6F. The secondary structures of the linkers in the fusions of (D) Tb-Tm and (E) Tm-Tb. The blue dashed line represents the H-bond. All images were generated by ChimeraX (version 1.7.1).

and Tm-Tb. Most Tb-Tm fused with ADH at N-terminus retained ADH activity indicating the proper oligomerization. In the case of Tm-Tb, fusing ADH at the C-terminus potentially disrupts the oligomerization interfaces between the subunits,[48] thus hindering the correct assembly of ADH to form a functional tetramer, and finally leading to a significant reduction or complete loss of ADH activity. The oligomerization disruption of ADHs by different fusion directions was also documented in other studies, resulting in activity loss.[50] The BN-PAGE analysis corroborated the structural changes by showcasing variations in oligomerization levels of different fusion enzymes (Figure 2).

A notable observation is how the conformations of the linkers change upon fusion. For example, the linker 6F (SRSAAG) displays predominantly flexible loops in Tb-6F-Tm, as expected, as it contains a 50% proportion of glycine (Gly) and serine (Ser) residues that naturally form unconstrained random coils to provide flexibility between enzyme domains (Figure 5C, left). However, the fusion orientation matters. For Tm-6F-Tb, the C-terminal Gly of 6F becomes part of the β-sheet 1 of *Tb*ADH, while the other end forms a short α-helix via the lateral interactions with the C-terminal Glu-Arg-Ala (535—537) motif of *Tm*CHMO, thereby introducing rigidity (Figure 5C, right). This arrangement may allow the fusion enzyme to achieve the required conformation for its existence while ensuring proximity between *Tb*ADH and *Tm*CHMO, but, at the same time, it compromises the oligomerization of *Tb*ADH. Similarly, the longer flexible linkers, 14F and 12F, form random loops with high flexibility in Tb-Tm (Figure 5D), while in Tm-Tb, they form a more pronounced and stiffer α-helix with the residues (525–541) at the end of *Tm*CHMO compared to 6F, highly limiting the spatial movement of both enzymes (Figure 5E). The rigid linkers, 6R2 and 6R3, show the intended rigidity in both Tb-Tm and Tm-Tb (Figure 5D,E). In addition, they form a helical structure with two complete turns, which may render ADH inactive. Not only does the fusion orientation and the linker flexibility profoundly affect the activity of the fusion enzyme, but the intrinsic structure of the protein also reciprocally affects the conformation of the linker. The structural conformation of the studied linkers corresponds to the catalytic property, the more flexible the linker, the more active the fusion enzyme.

To further unravel the flexibility of the fusion enzymes, the MD simulations were performed for the selected linkers and analyzed regarding the root-mean-square fluctuations (RMSF) (Figure 6), with additional replicas shown in Figure S3 and root-mean-square deviations (RMSD) (Figure S4). Intriguingly, MD simulations showed that the averaged flexibility of *Tb*ADH in the fusion enzymes changed drastically compared to the single enzyme, especially in the specific region of residues 97–104 (Figure 6A,B). This region was found to be located at the entrance to the active pocket and involved in substrate recognition, as well as assisting substrate access to the active site.[49] Upon closer inspection in more active Tb-Tm fusion enzymes, averaged RMSF values in this region were followed in the order of 6F > 14F > 6R3 > 12F (Figure 6A), suggesting improved substrate binding and orientation, aligning with the experimental observations of specific activities (Figure 1B). In contrast, no significant flexibility change of this region was observed for Tm-Tb that were less active (Figure 6B). Compared to *Tb*ADH, the RMSF values for *Tm*CHMO remained constantly stable, suggesting the fusion enzymes are not significantly affected by either linker properties or fusion orientation concerning CHMO activity (Figure 6C). As for the linkers themselves, the longer flexible linker 14F induced the highest RMSF and RMSD values (Figure 6D and Figure S4), implying a greater degree of movement and conformational changes for both enzymes. Conversely, the short rigid linker 6R2 led to lower RMSF values, indicating a more rigid structure that restricts the movement between the fused enzymes. These findings are consistent with the experiment analyses of the activities.

In addition to enzyme flexibility, the distance between the active sites of the fused two enzymes can play a pivotal role in the catalytic efficiency due to the altered reactant transportation. Therefore, the distance between the active sites of *Tb*ADH (His59 and Asp150) and *Tm*CHMO (Asp59 and Arg329) were calculated from MD simulations (Figure 7A). A closer distance was noted in Tb-14F-Tm (52 Å) and Tb-6F-Tm (51 Å) (Figure 7B), which may favor to shorten thetransfer path of the intermediates CHO and NADPH regenerated by ADH to CHMO. Therefore, it seems that the flexible glycine linkers are envisioned to be more favorable to maintain the flexibility of both enzymes and shorten the diffusion distance of intermediates. Surprisingly, Tm-6R2-Tb with the small-size linker displayed the farthest distance of 73 Å. These findings suggest

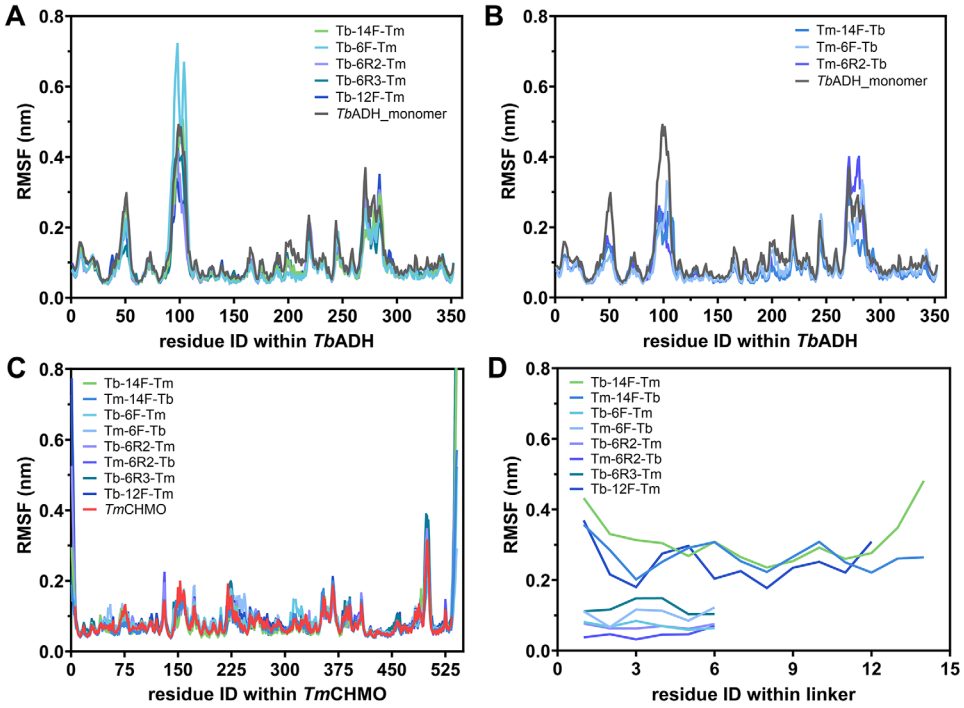

Figure 6. Averaged root-mean-square fluctuations (RMSF) of the Cα-atoms from MD simulations for (A) the single and fused *Tb*ADH in Tb-Tm, (B) the single and fused *Tb*ADH in Tm-Tb, (C) the single and fused *Tm*CHMO in fusions, and (D) the linkers.

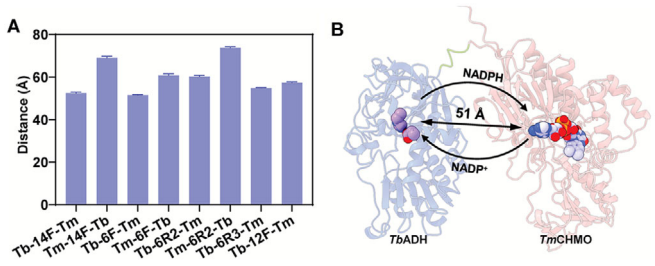

Figure 7. (A) The averaged distance between the active sites of *Tb*ADH and *Tm*CHMO. (B) View of labeled minimum distances between the active sites of *Tb*ADH and *Tm*CHMO in Tb-6F-Tm.

that shorter linkers do not necessarily lead to closer proximities of fusion enzymes per se (individual enzyme), and the flexibility of the linker can highly influence the arrangement of the fused enzymes. This contradicts the intuitive assumption that reducing the length of linkers spontaneously shortens the distance between the active sites of fused enzymes, thereby enhancing substrate transfer efficiency. Instead, linkers' flexibility and structural compatibility are paramount in determining the spatial arrangement of fusion enzymes,[50] underscoring the significance of rational linker design in achieving desired enzyme activity.

A detailed analysis of the mean smallest distance between all residues within the individual enzymes and their respective fusion constructs was performed to better understand the interactions between the monomers upon fusion (Figures S5–S15). Notably, the strength of these interactions was highly dependent on the sequence orientation, with significant interactions observed only when *Tb*ADH was positioned at the N-terminus, particularly in the construct Tb-6F-Tm (Figure S10), Tb-6R3-Tm (Figure S14), and Tb-12F-Tm (Figure S15). This finding aligns with experimental results demonstrating a complete loss of *Tb*ADH activity when fused at the C-terminus. Additionally, visualizations of the linkers and their hydrogen-bonding (HB) networks with both enzymes provide further structural insights into their flexibility (Figures S16 and S17). In general, an extensive HB network within the linker can reduce flexibility, potentially affecting substrate accessibility and enzyme dynamics.[51] The HB network analysis revealed that when *Tb*ADH was positioned at the C-terminus, particularly in the construct Tm-6R2-Tb, the highest number of HB interactions were observed, explaining its reduced flexibility and diminished activity.

2.6. The Cascade Reaction of Fusion Enzymes in Biphasic Systems

To explore the potential of the fusion enzymes, the optimal fusion constructs (Tb-6F-Tm, Tb-12F-Tm, and Tb-14F-Tm) were evaluated in a biphasic system containing KPi buffer and 50 vol.% cyclopentyl methyl ether (CPME), with the progressive curves shown in Figure 8 and mass balance in Figure S18. Herein, CPME was chosen as it is recognized as an eco-friendly solvent[52] and has documented superior performance for biocatalytic reactions.[17,25] The results show that ECL progressively accumulates more than pure buffer in the biphasic system over a longer reaction time (144 h) (Figure 8D). This highlights the importance of introducing organic media for this reaction, as the extraction of the lactone to CPME in the biphasic system minimized the auto–hydrolysis of ECL.[53]

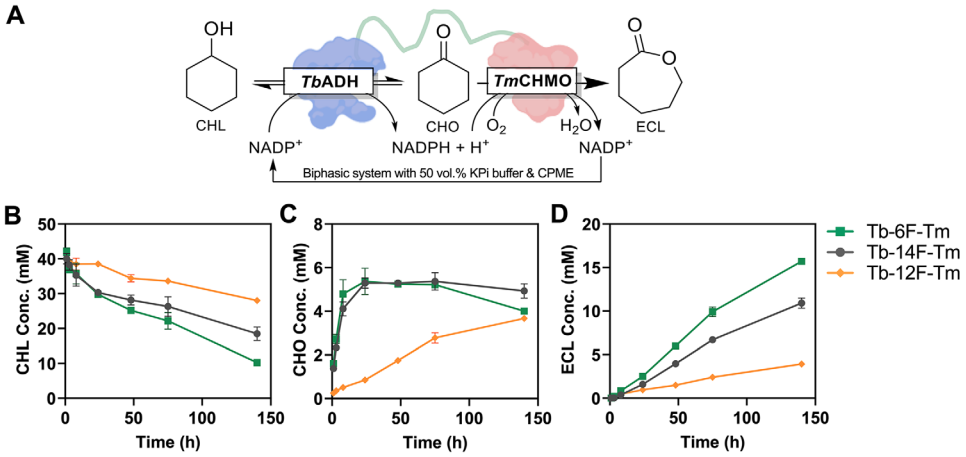

Figure 8. Progressive curves of (A) CHL, (B) CHO, and (C) ECL in biphasic systems with 50 vol.% cyclopentyl methyl ether (CPME). Reaction condition: 2 mL KPi system (50 mM, pH 8.0) or 5 mL biphasic system with 40 mM CHL, 1 mM $NADP^+$, 1 U/mL CHMO activity, and varying ADH activity, at 30 °C and 480 rpm.

In detail, Tb-6F-Tm gave rise to the highest ECL concentration (15.7 mM), which is 2.7 times of aqueous medium. Following Tb-6F-Tm, Tb-14F-Tm achieved a 1.4-fold increase in ECL formation (10.9 mM), while Tb-12F-Tm was the least efficient. The catalytic performance of these fusion enzymes regarding ECL formation aligns with their respective ADH/CHMO activity ratios (6F, 14F, 12F, 2.2 > 0.8 > 0.2). With the same CHMO activity, a higher ADH activity led to a higher CHO accumulation; however, much of which was extracted to the organic phase, thus mitigating the CHO inhibition on CHMO.[29] These findings are in contrast to the studies in aqueous media, where the optimal activity ratio of ADH/CHMO was reported to be 1:3 for purified single enzymes[54] and 1:10 for the enzymes in whole cells.[47] In aqueous media, a higher CHMO activity is preferred to accelerate the oxidation of CHO to form ECL, which in turn abates the CHO inhibition but intensifies ECL inhibition on CHMO. The use of aqueous–organic biphasic systems can overcome all these inhibitory effects thanks to the altered partitioning of all reactants, hence enhancing overall reaction efficiency. In summary, the selected fusion enzymes functioned well in biphasic systems and led to improved ECL productivity following the order of Tb-6F-Tm, Tb-14F-Tm, and Tb-12F-Tm. This trend aligns with MD simulations showing that the 6F linker minimized the active-site distance between the fused enzymes reducing intermediate diffusion by facilitating direct substrate transfer. In addition to the activity ratio of ADH/CHMO, the "reactant channeling" between the enzyme domains of fusion enzymes is assumed to play a significant role, which is determined by the structural conformations of linkers and fusion enzymes and thus needs to be further investigated in depth.

Overall, the obtained experimental and computational results provide compelling evidence to support the catalytic superiority of the fusion enzymes with the flexible linkers. These findings are consistent with the previous studies that compared the enzyme activity and catalytic efficiency of oxidoreductases fused by flexible[19,24] and rigid linkers.[31,55] Some discrepancies can be attributed to several factors, including specific enzyme pairings and target reactions. The intricate interplay between these variables exerts a significant influence on the overall catalytic performance of fusion enzymes. Nevertheless, the exploration of suitable peptide linkers for fusion enzymes to offer superior catalytic properties is worthwhile but still challenging.

3. Conclusion

This study targeted the intricate challenge of designing fusion enzymes through a combination of experiments and simulations, emphasizing the impact of fusion orientation and the need to strike a delicate balance between flexibility and rigidity by selecting suitable linkers. Twelve novel fusion enzymes of *Tm*CHMO and *Tb*ADH with various linkers in two directions were constructed and assessed regarding their catalytic performance. *Tm*CHMO retained its activity across all the fusion enzymes, while *Tb*ADH was inactivated in some specific cases, especially when fused at the C-terminus. Due to its intrinsic tetrameric structure, *Tb*ADH is more susceptible to the effects of linkers. Specifically, the rigid linkers (e.g., 6R2) enhance the thermal stability of *Tb*ADH, but at the same time reduce activity by compromising structural flexibility or steric adaptability due to the formation of α-helical structures. The flexible linkers (e.g., 6F and 14F) form random coil structures that benefit the flexibility of the critical region at N-terminus and substrate accessibility, thereby improving catalytic efficiency. Significantly, the conformations of linker and fusion enzymes mutually influence each other, thus affecting the proximity of the active sites and flexibility of the two enzymes. Furthermore, applying the optimal fusion enzymes in the linear cascade reaction for synthesizing ε-caprolactone using both aqueous and biphasic systems with 50 vol.% CPME, demonstrates the potential advantages of combining fusion enzymes with nonconventional media.

In summary, this study underscores the importance of integrating empirical research with computational strategies when designing fusion enzymes, shedding light on optimizing catalytic efficiency in biotechnological applications. Careful design

of such bifunctional enzymes has proved challenging, both to optimize stability and promote effective channeling of substrates and cofactors within the fusion complex. In addition, a comprehensive investigation involving different nonconventional media and varied reaction conditions is imperative for future studies.

Supporting Information

The authors have cited additional references within the Supporting Information.[56–78]

Acknowledgements

The authors acknowledge Deutsche Forschungsgemeinschaft (DFG; Grant No. 391127961), Aarhus Universitets Forskningsfond (AUFF Grant No. AUFF-T-2018-7-11), and China Scholarship Council (CSC Grant No. 202108610066) for the financial support. The authors thank Dr. Friso Aalbers and Prof. Dr. Marco Fraaije (University of Groningen, The Netherlands) for kindly providing the plasmid for the fusion enzyme of Tb-14F-Tm. The authors extend thanks to Dr. Sven Jakobtorweihen (Hamburg University of Technology) for his support and guidance in conducting the MD simulations. The authors gratefully acknowledge the computing time granted by the Resource Allocation Board and provided on the supercomputers at NHR@ZIB and NHR@Göttingen under the project hhi00040. The authors would also like to thank B.Sc. Kartsen Georgi and M.Sc. Michael Romain for the experiments and results obtained as part of their thesis studies.

Conflict of Interests

The authors declare no conflict of interest.

Data Availability Statement

The data that support the findings of this study are available from the corresponding author upon reasonable request.

Keywords: Biocatalytic cascades · Baeyer–Villiger monooxygenases · Fusion enzymes · Linker design · Molecular dynamics simulations

[1] E. Ricca, B. Brucher, J. H. Schrittwieser, *Adv. Synth. Catal.* **2011**, *353*, 2239–2262.
[2] D. Wu, X. Lei, *Tetrahedron* **2022**, *127*, 133099–133111.
[3] C. Scherkus, S. Schmidt, U. T. Bornscheuer, H. Gröger, S. Kara, A. Liese, *Biotechnol. Bioeng.* **2017**, *114*, 1215–1221.
[4] H. Leisch, K. Morley, P. C. K. Lau, *Chem. Rev.* **2011**, *111*, 4165–4222.
[5] M. Delgove, M. Elford, K. Bernaerts, S. Wildeman, *J. Chem. Technol. Biotechnol.* **2018**, *93*, 2131–2140.
[6] J. Engel, K. S. Mthethwa, D. J. Opperman, S. Kara, *Mol. Catal.* **2019**, *468*, 44–51.
[7] J. Preissler, H. A. Reeve, T. Zhu, J. Nicholson, K. Urata, L. Lauterbach, L. L. Wong, K. A. Vincent, O. Lenz, *ChemCatChem* **2020**, *12*, 4853–4861.
[8] M. L. Mascotti, W. J. Lapadula, M. J. Ayub, *PLOS One* **2015**, *10*, e0132689–e0132705.
[9] A. Delavault, K. Ochsenreither, C. Syldatk, *Phys. Sci. Rev.* **2024**, *9*, 2875–2897.
[10] G. Vernet, M. Hobisch, S. Kara, *Curr. Opin. Green Sustain. Chem.* **2022**, *38*, 100692–100699.
[11] G. de Gonzalo, M. D. Mihovilovic, M. W. Fraaije, *ChemBioChem* **2010**, *11*, 2208–2231.
[12] L. Huang, P. de Dominguez Maria, S. Kara, *Chem. Oggi-Chem. Today* **2018**, *36*, 48–56.
[13] M. V. van Schie, J. Spöring, M. Bocola, P. D. de María, D. Rother, *Green Chem.* **2021**, *23*, 3191–3206.
[14] H. Ramesh, T. Mayr, M. Hobisch, S. Borisov, I. Klimant, U. Krühne, J. M. Woodley, *J. Chem. Technol. Biotechnol.* **2016**, *91*, 832–836.
[15] F. Tieves, F. Tonin, E. Fernández-Fueyo, J. M. Robbins, B. Bommarius, A. S. Bommarius, M. Alcalde, F. Hollmann, *Tetrahedron* **2019**, *75*, 1311–1314.
[16] D. Holtmann, F. Hollmann, *Mol. Catal.* **2022**, *517*, 112035–112039.
[17] G. Vernet, Y. Ma, N. Zhang, S. Kara, *ChemBioChem* **2023**, *24*, e202200794.
[18] S. Schmidt, U. T. Bornscheuer, in *The Enzymes*, Elsevier, Amsterdam, **2020**, pp. 231–281.
[19] A. Kokorin, V. B. Urlacher, *ChemBioChem* **2022**, *23*, e202200065.
[20] F. S. Aalbers, M. W. Fraaije, *Appl. Microbiol. Biotechnol.* **2017**, *101*, 7557–7565.
[21] J. Jung, J. Braun, T. Czabany, B. Nidetzky, *ChemBioChem* **2020**, *21*, 1534–1543.
[22] M. J. Kummer, Y. S. Lee, M. Yuan, B. Alkotaini, J. Zhao, E. Blumenthal, S. D. Minteer, *JACS Au.* **2021**, *1*, 1187–1197.
[23] N. Beyer, J. K. Kulig, A. Bartsch, M. A. Hayes, D. B. Janssen, M. W. Fraaije, *Appl. Microbiol. Biotechnol.* **2017**, *101*, 2319–2331.
[24] E.-Y. Jeon, A.-H. Baek, U. T. Bornscheuer, J.-B. Park, *Appl. Microbiol. Biotechnol.* **2015**, *99*, 6267–6275.
[25] L. Huang, F. S. Aalbers, W. Tang, R. Röllig, M. W. Fraaije, S. Kara, *ChemBioChem* **2019**, *20*, 1653–1658.
[26] Á. Mourelle-Insua, F. S. Aalbers, I. Lavandera, V. Gotor-Fernández, M. W. Fraaije, *Tetrahedron* **2019**, *75*, 1832–1839.
[27] Y. Ma, G. Vernet, N. Zhang, S. Kara, *ChemCatChem* **2025**, *17*, 1–8.
[28] X. Chen, J. Zaro, W.-C. Shen, *Adv. Drug Delivery Rev.* **2013**, *65*, 1357–1369.
[29] D. T. Monterrey, I. Ayuso-Fernández, I. Oroz-Guinea, E. García-Junceda, *Biotechnol. Adv.* **2022**, *60*, 108016–108034.
[30] Y. Ma, N. Zhang, G. Vernet, S. Kara, *Front. Bioeng. Biotechnol.* **2022**, *10*, 944226–944237.
[31] J. Guo, Z. Cheng, J. Berdychowska, X. Zhu, L. Wang, L. Peplowski, Z. Zhou, *Int. J. Biol. Macromol.* **2021**, *181*, 444–451.
[32] M. L. Corrado, T. Knaus, F. G. Mutti, *ChemBioChem* **2018**, *19*, 679–686.
[33] F. S. Aalbers, M. W. Fraaije, *ChemBioChem* **2019**, *20*, 20–28.
[34] S. M. Richardson, P. M. Marchetti, M. A. Herrera, D. J. Campopiano, *ACS Catal.* **2022**, *12*, 12701–12710.
[35] Y. Li, P. Luan, L. Dong, J. Liu, L. Jiang, J. Bai, F. Liu, Y. Jiang, *G. Synth. Catal.* **2024**, *5*, 80–87.
[36] J. Jumper, R. Evans, A. Pritzel, T. Green, M. Figurnov, O. Ronneberger, K. Tunyasuvunakool, R. Bates, A. Žídek, A. Potapenko, A. Bridgland, C. Meyer, S. A. A. Kohl, A. J. Ballard, A. Cowie, B. Romera-Paredes, S. Nikolov, R. Jain, J. Adler, T. Back, S. Petersen, D. Reiman, E. Clancy, M. Zielinski, M. Steinegger, M. Pacholska, T. Berghammer, S. Bodenstein, D. Silver, O. Vinyals, A. W. Senior, K. Kavukcuoglu, P. Kohli, D. Hassabis, *Nature* **2021**, *596*, 583–589.
[37] T. Tsaban, J. K. Varga, O. Avraham, Z. Ben-Aharon, A. Khramushin, O. Schueler-Furman, *Nat. Commun.* **2022**, *13*, 176–188.
[38] R. Evans, M. O'Neill, A. Pritzel, N. Antropova, A. Senior, T. Green, A. Žídek, R. Bates, S. Blackwell, J. Yim, O. Ronneberger, S. Bodenstein, M. Zielinski, A. Bridgland, A. Potapenko, A. Cowie, K. Tunyasuvunakool, R. Jain, E. Clancy, P. Kohli, J. Jumper, D. Hassabis, BioRxiv. **2022**, https://doi.org/10.1101/2021.10.04.463034.
[39] P. Bryant, G. Pozzati, A. Elofsson, *Nat. Commun.* **2022**, *13*, 1265–1276.
[40] I. Johansson-Åkhe, B. Wallner, *Front. Bioinforma.* **2022**, *2*, 959160.
[41] A. Gran-Scheuch, F. Aalbers, Y. Woudstra, L. Parra, M. W. Fraaije, in *Methods Enzymol* **2021**, Elsevier, Amsterdam, pp. 107–143.
[42] D. E. Torres Pazmiño, R. Snajdrova, B.-J. Baas, M. Ghobrial, M. D. Mihovilovic, M. W. Fraaije, *Angew. Chem. Int. Ed Engl.* **2008**, *47*, 2275–2278.

[43] T. Heine, K. Tucker, N. Okonkwo, B. Assefa, C. Conrad, A. Scholtissek, M. Schlömann, G. Gassner, D. Tischler, *Appl. Biochem. Biotechnol.* **2017**, *181*, 1590–1610.
[44] E. Romero, J. R. G. Castellanos, A. Mattevi, M. W. Fraaije, *Angew. Chem., Int. Ed.* **2016**, *55*, 15852–15855.
[45] R. J. Lamed, E. Keinan, J. G. Zeikus, *Enzyme Microb. Technol.* **1981**, *3*, 144–148.
[46] D. R. Breiter, E. Resnik, L. J. Banaszak, *Protein Sci. Publ. Protein Soc.* **1994**, *3*, 2023–2032.
[47] S. Schmidt, C. Scherkus, J. Muschiol, U. Menyes, T. Winkler, W. Hummel, H. Gröger, A. Liese, H.-G. Herz, U. T. Bornscheuer, *Angew. Chem. Int. Ed.* **2015**, *54*, 2784–2787.
[48] Y. Korkhin, A. Joseph, M. Peretz, O. Bogin, Y. Burstein, F. Frolow, *Protein Sci.* **1999**, *8*, 1241–1249.
[49] C. Li, J. Heatwole, S. Soelaiman, M. Shoham, *Proteins Struct. Funct. Bioinforma.* **1999**, *37*, 619–627.
[50] Y. Li, P. Luan, L. Dong, J. Liu, L. Jiang, J. Bai, F. Liu, Y. Jiang, *G. Synth. Catal.* **2024**, *5*, 80–87.
[51] A.-C. C. Carlsson, M. R. Scholfield, R. K. Rowe, M. C. Ford, A. T. Alexander, R. A. Mehl, P. S. Ho, *Biochemistry* **2018**, *57*, 4135–4147.
[52] G. de Gonzalo, A. R. Alcántara, P. de Domínguez María, *ChemSusChem* **2019**, *12*, 2083–2097.
[53] S. Kara, D. Spickermann, J. H. Schrittwieser, A. Weckbecker, C. Leggewie, I. W. C. E. Arends, F. Hollmann, *ACS Catal.* **2013**, *3*, 2436–2439.
[54] H. Mallin, H. Wulf, U. T. Bornscheuer, *Enzyme Microb. Technol.* **2013**, *53*, 283–287.
[55] Y. Zhang, Y. Wang, S. Wang, B. Fang, *Eng. Life Sci.* **2017**, *17*, 989–996.
[56] I. Wittig, H.-P. Braun, H. Schägger, *Nat. Protoc.* **2006**, *1*, 418–428.
[57] J. Huang, S. Rauscher, G. Nawrocki, T. Ran, M. Feig, B. L. de Groot, H. Grubmüller, A. D. MacKerell, *Nat. Methods* **2017**, *14*, 71–73.
[58] A. D. MacKerell, D. Bashford, M. Bellott, R. L. Dunbrack, J. D. Evanseck, M. J. Field, S. Fischer, J. Gao, H. Guo, S. Ha, D. Joseph-McCarthy, L. Kuchnir, K. Kuczera, F. T. K. Lau, C. Mattos, S. Michnick, T. Ngo, D. T. Nguyen, B. Prodhom, W. E. Reiher, B. Roux, M. Schlenkrich, J. C. Smith, R. Stote, J. Straub, M. Watanabe, J. Wiórkiewicz-Kuczera, D. Yin, M. Karplus, *J. Phys. Chem. B* **1998**, *102*, 3586–3616.
[59] S. R. Durell, B. R. Brooks, A. Ben-Naim, *J. Phys. Chem.* **1994**, *98*, 2198–2202.
[60] S. Jo, T. Kim, V. G. Iyer, W. Im, *J. Comput. Chem.* **2008**, *29*, 1859–1865.
[61] J. Lee, X. Cheng, J. M. Swails, M. S. Yeom, P. K. Eastman, J. A. Lemkul, S. Wei, J. Buckner, J. C. Jeong, Y. Qi, S. Jo, V. S. Pande, D. A. Case, C. L. Brooks, A. D. MacKerell, J. B. Klauda, W. Im, *J. Chem. Theory Comput.* **2016**, *12*, 405–413.
[62] J. Lee, M. Hitzenberger, M. Rieger, N. R. Kern, M. Zacharias, W. Im, *J. Chem. Phys.* **2020**, *153*, 035103.
[63] S. Jo, X. Cheng, S. M. Islam, L. Huang, H. Rui, A. Zhu, H. S. Lee, Y. Qi, W. Han, K. Vanommeslaeghe, A. D. MacKerell, B. Roux, W. Im, in *Adv. Protein Chem. Struct. Biol.* (Ed.: T. Karabencheva-Christova), Academic Press, Cambrige, MA **2014**, pp. 235–265.
[64] S.-J. Park, N. Kern, T. Brown, J. Lee, W. Im, *J. Mol. Biol.* **2023**, *435*, 167995.
[65] T. Darden, D. York, L. Pedersen, *J. Chem. Phys.* **1993**, *98*, 10089–10092.
[66] B. Hess, H. Bekker, H. J. C. Berendsen, *J. Comput. Chem.* **1997**, *18*, 1463.
[67] S. Miyamoto, P. A. Kollman, *J. Comput. Chem.* **1992**, *13*, 952–962.
[68] M. J. Abraham, T. Murtola, R. Schulz, S. Páll, J. C. Smith, B. Hess, E. Lindahl, *SoftwareX* **2015**, *1–2*, 19–25.
[69] M. J. Abraham, D. van der Spoel, E. Lindahl, B. Hess, the GROMACS development team, GROMACS User Manual Version **2019**.
[70] H. Bekker, H. Berendsen, E. Dijkstra, S. Achterop, R. Vondrumen, D. Vanderspoel, A. Sijbers, H. Keegstra, M. Renardus, in Methods in computational physics, World Scientific Publishing, Singapore **1992**, pp. 252–256.
[71] L. Martínez, R. Andrade, E. G. Birgin, J. M. Martínez, *J. Comput. Chem.* **2009**, *30*, 2157–2164.
[72] N. Zhang, J. P. Bittner, M. Fiedler, T. Beretta, P. de Domínguez María, S. Jakobtorweihen, S. Kara, *ACS Catal.* **2022**, *12*, 9171–9180.
[73] R. W. Hockney, *Methods Comput Phys.* **1970**, *9*, 135–211.
[74] G. Bussi, D. Donadio, M. Parrinello, *J. Chem. Phys.* **2007**, *126*, 014101.
[75] H. J. C. Berendsen, J. P. M. Postma, W. F. van Gunsteren, A. DiNola, J. R. Haak, *J. Chem. Phys.* **1984**, *81*, 3684–3690.
[76] M. Vassaux, S. Wan, W. Edeling, P. V. Coveney, *J. Chem. Theory Comput.* **2021**, *17*, 5187–5197.
[77] B. Knapp, L. Ospina, C. M. Deane, *J. Chem. Theory Comput.* **2018**, *14*, 6127–6138.
[78] M. Parrinello, A. Rahman, *J. Appl. Phys.* **1981**, *52*, 7182–7190.

Manuscript received: November 15, 2024
Revised manuscript received: January 31, 2025
Accepted manuscript online: March 9, 2025
Version of record online: ■■, ■■